Yang HAN[1], Lin XU[2]

University of Electronic Science and Technology of China (1), Shanghai JiaoTong University (2)

Averaged and switching function modelling for the active power filter with LCL-type coupling impedance

Abstract. *This paper presents the averaged and switching function modelling for the active power filter (APF) with LCL-type coupling impedance. The mathematical model of the LCL-type APF is derived using switching function modelling technique, followed by the Fourier series analysis of the switching functions. The equivalent circuits are presented from the averaged and switching ripple model. The presented technique is also extended to the analysis of the modulation signal and inverter dc-link voltage. Finally, the experimental results are presented for verification.*

Streszczenie. *Artykuł prezentuje modelowanie uśredniającej i przełączającej funkcji aktywnego filtru z impedancja sprzęgającą typu LCL. Model matematyczny jest wyprowadzony przy modelowaniu funkcji przełączającej a następnie przez analizę Fouriera tej funkcji. Zaprezentowano schemat zastępczy. Przedstawiona technika może być rozszerzona do analizy sygnału modulowanego i przekształtnika. Na zakończenie przedstawiono wyniki eksperymentów. (**Modelowanie funkcji uśredniania i przełączania w aktywnym filtrze z impedancją sprzęgającą typu LCL**)*

Keywords: Active power filter, averaged model, switching function, switching ripple model, LCL-filter
Słowa kluczowe: filtry aktywne, filtr LCL, funkcja uśredniania..

I. Introduction

In recent years, the power quality issues have received considerable attention due to the proliferation of nonlinear loads, which causes power loss, voltage sag/swell and temporary interruptions [1, 2]. To mitigate these problems, the active power filters (APFs) are utilized to compensate harmonic current and improve power factor. Extensive research was carried out concerning the circuit topologies, harmonic detection methods, current controller design methods of the APFs [3-6].

However, the stringent theoretical modelling of the APFs was not reported in the literature. This paper aims to cover this gap and presents the strict theoretical modelling of the APF with LCL-type coupling impedance using switching function modelling method. The mathematical model of the APF is derived using switching functions, and the averaged and switching ripple equivalent circuits are obtained by exploiting the Fourier series expansion of the switching functions. Next, the ac-side and the dc-side model of the inverter are reported, followed by the strict derivation of the averaged and switching models for the modulation signal as well as the inverter dc-link voltage.

The organization of this paper is as follows. Secition II presents the general description of the LCL-type APF. Section III presents the switching function model of the LCL-type APF. Sections IV and V presents the averaged and swithing model of the ac-side and dc-side of the inverter, respectively. Next, Sections VI and VII present the analysis of modulation signal and the dc-link fluctuation . Section VIII presents the experimental results. Finally, Section IX concludes this paper.

II. General Description of the LCL-type APF

Fig.1 shows the circuit diagram of the shunt APF with LCL-type coupling impedance. To derive the averaged and switching function model of the converter, the following assumptions are considered [1, 4, 5]:

(1).The equivalent resistance of the inductors L_g and L_c are neglected; (2).The switching devices, i.e., the IGBTs, are ideal switch, which implies the instantaneous switching transistions between 'on' and 'off' states and the deadtime is also neglected; (3).The grid is represented using Thevenin's equivalent circuit, i.e., the ideal voltage source in series with effective resistance R_s and inductance L_s; (4). The nonlinear load is denoted by the controlled current source (CCS); (5).The pulse-width modulation (PWM) process is within its linear region, i.e., the peak of the modulation signal is always lower than the peak of carrier signal. Based on the aforementioned assumptions, the swithing function model of the LCL-type APF would be derived in the forthcoming subsections. In the next Section, the switching function model of the LCL-type APF would be presented.

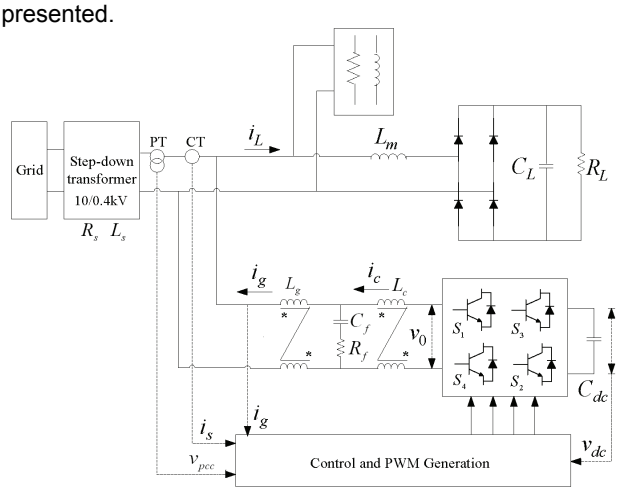

Fig.1 Circuit diagram of the shunt APF with LCL output filter (Only phase A is shown).

III. Switching Function Model of the LCL-type APF

The switching states of the IGBT can be denoted by '1' and '0', representing the 'on' and 'off' state of the switch. The switching states of the two IGBTs from the same phase leg are complementary to each other. Hence the switching states of the upper switches (S_1 and S_3) can be utilized to denote the state of the converter. The output voltage of the inverter can be represendted by the switching functions S_1, S_3 and the dc-link voltage v_{dc} of the inverter, as [1,4-6]:

$$v_0 = \left[S_1(t) - S_3(t)\right] v_{dc}(t) \tag{1}$$

Hence, the IGBT currents i_{S1}~i_{S4} can be denoted as:

$$i_{S_1}(t) = S_1(t) i_c(t), i_{S_4}(t) = \left[1 - S_1(t)\right] i_c(t) \tag{2}$$

$$i_{S_3}(t) = -S_3(t) i_c(t), i_{S_2}(t) = \left[1 - S_3(t)\right] i_c(t) \tag{3}$$

where i_c denotes the output current of the inverter.

From Fig.1, the dc-link current of the inverter i_d can be represented as [4, 6]:

(4) $$i_d(t) = -\left[i_{S_1}(t) + i_{S_3}(t)\right] = \left[S_3(t) - S_1(t)\right] i_c(t)$$

From Eq.(1) and Eq.(4), the ac-side and the dc-side equivalent circuit of the converter can be easily derived. In this study, the ac-side converter is represented by the controlled voltage source (CVS) v_0, and the dc-side of the converter is denoted by controlled current source (CCS) i_d. Since the switching functions are discontinuous, the Fourier series expansion of the variable v_0 and i_d during one control cycle T_{sw} should be analyzed. Without lose of generality, the Fourier series expansion of the variable $y(t)$ within one cycle T_{sw} can be represented as [6]:

(5) $$\begin{aligned} y(t) &= \bar{y}(t) + y^{sw}(t) \\ &= \bar{y}(t) + \sum_{n=1}^{\infty} A_n(t)\sin(n\frac{2\pi}{T_{sw}}t) + \sum_{n=1}^{\infty} B_n(t)\cos(n\frac{2\pi}{T_{sw}}t) \end{aligned}$$

where the average component of $y(t)$ is denoted as:

(6) $$\bar{y}(t) = \frac{1}{T_{sw}}\int_{t-T_{sw}}^{t} y(\tau)d\tau$$

In addition, the switching ripple component is denoted by $y^{sw}(t)$, which represents the sum of the trigonometric functions, and the Fourier series components A_n and B_n can be derived as [6]:

(7) $$A_n(t) = \frac{2}{T_{sw}}\int_{t-T_{sw}}^{t} y(\tau)\sin(n\frac{2\pi}{T_{sw}}\tau)d\tau, n = 1,2,3,...$$

(8) $$B_n(t) = \frac{2}{T_{sw}}\int_{t-T_{sw}}^{t} y(\tau)\cos(n\frac{2\pi}{T_{sw}}\tau)d\tau, n = 1,2,3,...$$

Similarly, the inverter ouput current i_c and dc-link voltage v_{dc} can be rewritten as:

(9) $$v_o(t) = \left\{\left[\overline{S_1}(t) + S_1^{sw}(t)\right] - \left[\overline{S_3}(t) + S_3^{sw}(t)\right]\right\}\left[\overline{v_{dc}}(t) + v_{dc}^{sw}(t)\right]$$

(10) $$i_d(t) = \left\{\left[\overline{S_3}(t) + S_3^{sw}(t)\right] - \left[\overline{S_1}(t) + S_1^{sw}(t)\right]\right\}\left[\overline{i_c}(t) + i_c^{sw}(t)\right]$$

where the average component of the inverter ouput current i_c and dc-link voltage v_{dc} during one switching period T_{sw} can be derived as:

(11a) $$\overline{v_o}(t) = \left[\overline{S_1}(t) - \overline{S_3}(t)\right]\overline{v_{dc}}(t)$$

(11b) $$\overline{i_d}(t) = \left[\overline{S_3}(t) - \overline{S_1}(t)\right]\overline{i_c}(t)$$

Since $i_c^{sw} << \overline{i_c}$ and $v_{dc}^{sw} << \overline{v_{dc}}$, the switching ripple components of i_c and v_{dc} can be neglected, hence the switching ripple component of the output voltage v_0 and the dc-link current i_d during one switching period can be simplified as:

(12a) $$v_o^{sw}(t) = \left[S_1^{sw}(t) - S_3^{sw}(t)\right]\overline{v_{dc}}(t)$$

(12b) $$i_d^{sw}(t) = \left[S_3^{sw}(t) - S_1^{sw}(t)\right]\overline{i_c}(t)$$

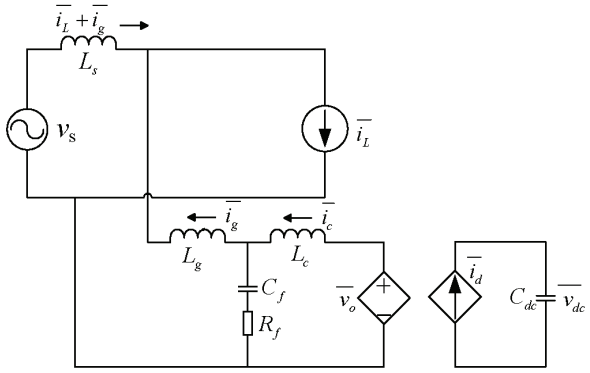

Fig. 2 Averaging model of the LCL-type APF

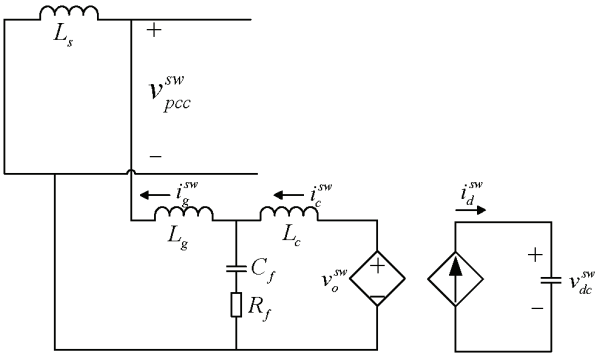

Fig. 3 Switching ripple model of the LCL-type APF

Assuming the grid voltage v_s and the load current i_L are free of switching ripple components, from the derivations obtained from Eq.(10) and Eq.(12), the circuit diagram in Fig.1 can be partitioned into two parts, namely, the averaged model and switching ripple model, as illustrated by Fig.2 and Fig.3, respectively.

From Fig.2, it can be noticed that the grid side is represented by voltage source v_s, the load is represented by the current source $\overline{i_L}$, the inverter and its dc-link are represented by controlled voltage source (CVS) $\overline{v_0}$ and controlled current source (CCS) $\overline{i_d}$. On the other hand, it can be observed from Fig.3 that the inverter and its dc-link are represented by controlled voltage source (CVS) v_0^{sw} and controlled current source (CCS) i_d^{sw}, and the load is open circuit.

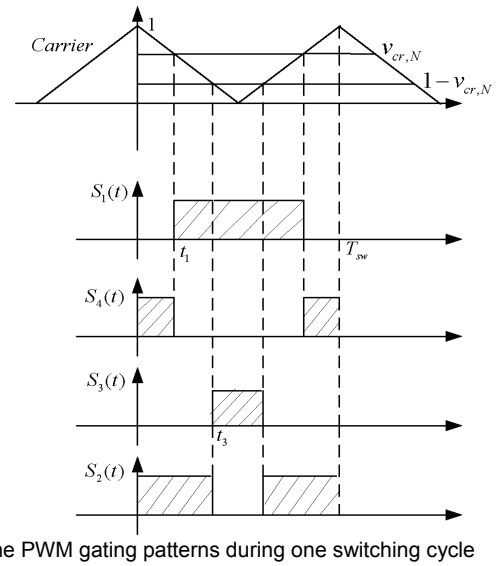

Fig. 4 The PWM gating patterns during one switching cycle

In order to derive the averaged and switching ripple components of each state variable, the Fourier analysis of the switching functions would be presented in the forthcoming derivations.

Fig.4 shows the switching patterns of the IGBTs and the modulation signal, the carrier signal during one control cycle. The carrier signal is a triangular waveform synthesized using the up-down counter, and the modulation signal of S_1 is denoted by $v_{cr,N}$, the modulation signal of S_3 is denoted by $(1\text{-}v_{cr,N})$. The modulation signals $v_{cr,N}$ and $(1\text{-}v_{cr,N})$ are compared with the triangular carriers to synthesize the gating signals for S_1 and S_3. Notably, the gating signals of S_4 and S_2 are complementary to those of S_1 and S_3. In Fig.4, t_1 and t_3 represents the instants when the switches S_1 and S_3 start conducting.

From Fig.4, the relations between the carrier signal and modulation signal can be derived as [4-6]:

$$\frac{T_{sw}-2t_1}{T_{sw}}=v_{cr,N},\ \frac{T_{sw}-2t_3}{T_{sw}}=1-v_{cr,N} \tag{13}$$

Hence, $t_1=T_{sw}(1\text{-}v_{cr,N})/2$, $t_3=T_{sw}v_{cr,N}/2$, and the average quantities of S_1 and S_3 within one switching cycle T_{sw} can be derived as:

$$\overline{S_1}(t)=\frac{1}{T_{sw}}\int_0^{T_{sw}}S_1(t)dt=v_{cr,N} \tag{14a}$$

$$\overline{S_3}(t)=\frac{1}{T_{sw}}\int_0^{T_{sw}}S_3(t)dt=1-v_{cr,N} \tag{14b}$$

Moreover, the switching ripple components of S_1 and S_3 within one switching cycle T_{sw} can be derived as:

$$\begin{aligned}S_i^{sw}(t)&=\sum_{n=1}^{\infty}A_{i,n}(t)\sin(n\frac{2\pi}{T_{sw}}t)\\&+\sum_{n=1}^{\infty}B_{i,n}(t)\cos(n\frac{2\pi}{T_{sw}}t)\quad(i=1,3)\end{aligned} \tag{15}$$

Furthermore, the modulation signal can be considered as constant during one switching cycle, and S_1, S_3 are even functions, hence $A_{1,n}=A_{3,n}$ holds. Thus the switching ripple component can be simplified as:

$$S_i^{sw}(t)=\sum_{n=1}^{\infty}B_{i,n}(t)\cos(n\frac{2\pi}{T_{sw}}t)\quad(i=1,3) \tag{16}$$

where

$$B_{1,n}(t)=-\frac{2}{n\pi}\sin\left\{n\pi\left[1-v_{cr,N}(t)\right]\right\} \tag{17a}$$

$$B_{3,n}(t)=-\frac{2}{n\pi}\sin\left[n\pi v_{cr,N}(t)\right] \tag{17b}$$

The aforementioned analysis presents the averaged and switching ripple components of the switching functions within one control cycle. Hence the averaged and switching ripple model of the LCL-type APF can be derived, which would be presented in the forthcoming subsections.

IV. Averaged and Switching Model of the Ac-Side

From Eqs.(10)-(14) and Fig.4, the average output voltage v_0 of the inverter can be derived as:

$$\overline{v_o}(t)=\left[2v_{cr,N}(t)-1\right]\overline{v_{dc}}(t)=\frac{v_{cr}(t)}{v_{dc}(t)}\overline{v_{dc}}(t) \tag{18}$$

Since $v_{dc}^{sw}<<\overline{v_{dc}}$, hence $v_{dc}(t)=\overline{v_{dc}}(t)$, $v_{cr}(t)=\overline{v_o}(t)$. From Fig.2 and according to the Kirchoff's Law, the following differential equation can be derived [1, 4, 6]:

$$\begin{cases}L_g\dfrac{d\overline{i_g}(t)}{dt}+L_c\dfrac{d\overline{i_c}(t)}{dt}=v_{cr}(t)-\overline{v_{pcc}}(t)\\ \overline{i_f}(t)=\overline{i_c}(t)-\overline{i_g}(t)=C_f\dfrac{d\overline{v_{cf}}(t)}{dt}\\ \overline{v_{cf}}(t)+R_f\overline{i_f}(t)=v_{cr}(t)-L_c\dfrac{d\overline{i_c}(t)}{dt}\end{cases} \tag{19}$$

From Eq.(18) and Eq.(19), the average output voltage of the voltage source inverter during one control cycle can be derived as:

$$\overline{v_0}(t)=v_{cr}(t)=\overline{v_{pcc}}(t)+L_g\frac{d\overline{i_g}(t)}{dt}+L_c\frac{d\overline{i_c}(t)}{dt} \tag{20}$$

where $\overline{v_{pcc}}(t)=e(t)-L_s\dfrac{d\overline{i_s}(t)}{dt}$. The aforementioned analysis lays the foundation for the steady-state analysis and the current controller design guidelines for the LCL-type APF. Substituting Eq.(15) into Eq.(12), we get:

$$v_o^{sw}(t)=-\sum_{n=1}^{\infty}\underbrace{\left\{\frac{4\overline{v_{dc}}(t)}{n\pi}\cos\frac{n\pi}{2}\sin\left[n\pi\frac{1-2v_{cr,N}(t)}{2}\right]\right\}}_{C_n(t)}\cdot\cos(n\frac{2\pi}{T_{sw}}t) \tag{21}$$

when n is odd number, we get $C_n(t)=0$, which implies that only even order switching ripple components remain in the inverter output voltage. From Fig.3, the relations between the inverter output current i_c and the switching ripple voltage can be denoted as:

$$v_o^{sw}=i_c^{sw}\cdot Z_{eq} \tag{22}$$

where Z_{eq} represents the equivalent impedance of the switching ripple model, which is represented by:

$$\begin{aligned}Z_{eq}&=R_{eq}+jX_{eq}\\&=jn\omega_{sw}L_c+jn\omega_{sw}(L_s+L_g)//(R_f+1/jn\omega_{sw}C_f)\end{aligned} \tag{23}$$

From Eq.(21) and Eq.(23), the switching ripple component of the output current is derived as:

$$\begin{aligned}i_c^{sw}(t)&=\sum_{n=1}^{\infty}\frac{R_{eq}}{R_{eq}^2+X_{eq}^2}C_n(t)\cos(n\frac{2\pi}{T_{sw}}t)\\&+\sum_{n=1}^{\infty}\frac{X_{eq}}{R_{eq}^2+X_{eq}^2}C_n(t)\cos(n\frac{2\pi}{T_{sw}}t-\frac{\pi}{2})\end{aligned} \tag{24}$$

Similarly, the switching ripple component of the grid voltage can be derived as:

$$v_{pcc}^{sw}(t)=K_s\frac{jn\omega_{sw}(L_s+L_g)//(R_f+1/jn\omega_{sw}C_f)}{jn\omega_{sw}(L_s+L_g)//(R_f+1/jn\omega_{sw}C_f)+jn\omega_{sw}L_c} \tag{25}$$

where $K_s=L_sv_c^{sw}(t)/(L_s+L_g)$.

V. Averaged and Switching Model of the Dc-Side

From Eqs.(10)-(14) and Fig.3, the average dc-link current i_d of the inverter can be derived as:

$$\overline{i_d}(t) = C_{dc}\frac{d\overline{v_{dc}}(t)}{dt} = (1-2V_{cr,N})\overline{i_c}(t) \tag{26}$$

Neglecting the switching ripple component, the dc-link voltage v_{dc} can be rewritten as:

$$\overline{v_{dc}}(t) = v_{dc}(t) = \overline{V_{dc}}(t) + \bar{v}_{dc,r}(t) \tag{27}$$

where $\overline{V_{dc}}$ denotes the average component of v_{dc}, and $\bar{v}_{dc,r}$ denotes the fluctuating component. It should be noted that the fluctuating component is directly related to the dc-link current, i.e., we have:

$$\bar{v}_{dc,r}(t) = \frac{1}{C_{dc}}\int \overline{i_d}(t)dt \tag{28}$$

where $\overline{i_d}(t) = -v_{cr}(t)\cdot\overline{i_c}(t)/\overline{v_{dc}}(t)$. Substituting Eq.(28) into Eq.(19), we get:

$$C_{dc}\overline{v_{dc}}(t)\frac{d\overline{v_{dc}}(t)}{dt} + \overline{v_{pcc}}(t)\overline{i_c}(t) + L_g\overline{i_c}(t)\frac{d\overline{i_g}(t)}{dt} + L_c\overline{i_c}(t)\frac{d\overline{i_c}(t)}{dt} = 0 \tag{29}$$

Subsituting Eq.(15) into Eq.(12), the ripple component of the dc-link current can be derived as:

$$i_d^{sw}(t) = \sum_{n=1}^{\infty}\underbrace{\frac{4\overline{i_c}(t)}{n\pi}\cos\frac{n\pi}{2}\sin\left[n\pi\cdot\frac{1-2V_{cr,N}(t)}{2}\right]}_{E_n(t)}\cos(n\frac{2\pi}{T_{sw}}t) \tag{30}$$

Hence, the switching ripple component of the dc-link voltage is derived as:

$$v_{dc}^{sw}(t) = \sum_{n=1}^{\infty}\underbrace{\frac{4\overline{i_c}(t)}{n^2\pi\omega_{sw}C_{dc}}\cos\frac{n\pi}{2}\sin\left[n\pi\cdot\frac{1-2V_{cr,N}(t)}{2}\right]}_{F_n(t)}\sin(n\frac{2\pi}{T_{sw}}t) \tag{31}$$

From Eq.(30) and Eq.(31), it can be noticed that when n is odd number, we have E_n=F_n=0, which implies that only even order switching ripple components remain in the dc-link voltage and current of the inverter. Besides, the magnitude of F_n is inversely proportional to n^2, indicating that the dc-link voltage ripple attenuates rapidly with the increase of harmonic order n.

VI. Analysis of the Modulation Signal

In order to achieve precise current tracking and stable dc-link voltage regulation of the inveter, the accurate generation of the modulation signal is the prerequisite. To simplify the anlsysis, the active current component of the APF is neglected, and the average component of the inverter current i_c and grid-side current i_g can be represented as:

$$\overline{i_x}(t) = I_{xq}\sin(\omega_1 t - \pi/2) + \sum_{h=2}^{H} I_{xh}\sin(h\omega_1 t - \varphi_{xh}), x = c, g \tag{32}$$

where I_{cq}, I_{ca} and I_{gq}, I_{gh} represent the amplitudes of reactive current and the individual harmonic component. Hence the inequalities I_{cq}≤I_{lq}, I_{ch}≤I_{lh}, I_{gq}≤I_{lq}, I_{gh}≤I_{lh} holds, where I_{lq} and I_{lh} denote the amplitdues of the reactive and harmonic component of load current.

Substituting Eq.(32) into Eq.(20), and assuming $\overline{v_{pcc}}(t) = V_{s1}\sin(\omega_1 t)$, we get:

$$\begin{aligned} v_{cr}(t) &= V_{s1}\sin(\omega_1 t) + \omega_1 I_{gq}L_g\cos(\omega_1 t - \pi/2) \\ &+ \sum_{h=2}^{H} h\omega_1 I_{gh}L_g\cos(h\omega_1 t - \varphi_{gh}) \\ &+ \omega_1 I_{cq}L_c\cos(\omega_1 t - \pi/2) \\ &+ \sum_{h=2}^{H} h\omega_1 I_{ch}L_c\cos(h\omega_1 t - \varphi_{ch}) \end{aligned} \tag{33}$$

Hence, the modulation signal $S(t)$ can be represented as:

$$S(t) = 2v_{cr,N}(t) - 1 = \frac{v_{cr}(t)}{\overline{v_{dc}}(t)} = \frac{v_{cr}(t)}{\overline{V_{dc}}(t) + \bar{v}_{dc,r}(t)} \tag{34}$$

For an arbitrary time instant, the inequality 0≤vcr,N≤1 holds, hence the following inequality holds:

$$v_{cr}(t) \le \overline{V_{dc}}(t) + \bar{v}_{dc,r}(t) \tag{35}$$

which provides the theoretical basis for dc-link voltage selection for the LCL-type APF.

Since $\bar{v}_{dc,r}(t) << \overline{V_{dc}}(t)$, hence inequality $\overline{v_{dc}}(t) \approx \overline{V_{dc}}(t)$ holds. Subsituting into Eq.(34), we get:

$$\begin{aligned} S(t) &= \left(m_e + m_q\right)\sin\omega_1 t + \sum_{h=2}^{H} m_{gh}\cos(h\omega_1 t - \varphi_{gh}) \\ &+ \sum_{h=2}^{H} m_{ch}\cos(h\omega_1 t - \varphi_{ch}) \end{aligned} \tag{36}$$

Equation (36) indicates that the modulation signal is not pure sinusoidal waveform. The variables me, mq, mgh, mch indicate the fundamental component of the grid voltage, reactive current, grid side and inverter side current with respect to the the dc-link voltage, which can be derived as:

$$\begin{aligned} m_e &= V_{s1}/\overline{V_{dc}} \\ m_q &= \omega_1(L_g I_{gq} + L_c I_{cq})/\overline{V_{dc}} \\ m_{gh} &= h\omega_1 L_g I_{gh}/\overline{V_{dc}} \\ m_{ch} &= h\omega_1 L_c I_{ch}/\overline{V_{dc}} \end{aligned} \tag{37}$$

VII. Analysis of the Dc-link Voltage Fluctuation

Subsituting Eq.(32) and Eq.(37) into Eq.(26), we get:

$$\begin{aligned} \overline{i_d}(t) = -&\left[\begin{aligned}&\left(m_e + m_q\right)\sin\omega_1 t + \sum_{h=2}^{H} m_{gh}\cos(h\omega_1 t - \varphi_{gh}) \\ &+ \sum_{h=2}^{H} m_{ch}\cos(h\omega_1 t - \varphi_{ch})\end{aligned}\right] \\ &\times\left[I_{cq}\sin(\omega_1 t - \pi/2) + \sum_{h=2}^{H} I_{ch}\sin(h\omega_1 t - \varphi_{ch})\right] \end{aligned} \tag{38}$$

After manipulation using trigonometric operations, the average dc-link current can be derived as:

$$\overline{i_d} = \overline{i}_{d,2} + \sum_{h=2}^{H}\overline{i}_{d,h+1} + \sum_{h=2}^{H}\overline{i}_{d,h-1} + \sum_{h=2}^{H}\overline{i}_{d,2h} + \sum_{\substack{h_1,h_2=2 \\ h_1<h_2}}^{H}\overline{i}_{d,h_1+h_2} + \sum_{\substack{h_1,h_2=2 \\ h_1<h_2}}^{H}\overline{i}_{d,h_2-h_1} \tag{39}$$

where

$$\overline{i}_{d,2}(t) = \frac{1}{2}(m_e + m_q) I_{cq} \sin(2\omega_1 t) \tag{40a}$$

$$\overline{i}_{d,h+1}(t) = \frac{1}{2}\left[(m_e + m_q) I_{ch} + m_{ch} I_{cq}\right]\cos\left[(h+1)\omega_1 t - \varphi_{ch}\right] + \frac{1}{2} I_{cq} m_{gh} \cos\left[(h+1)\omega_1 t - \varphi_{gh}\right] \tag{40b}$$

$$\overline{i}_{d,h-1}(t) = \frac{1}{2}\left[-(m_e + m_q) I_{ch} + m_{ch} I_{cq}\right]\cos\left[(h-1)\omega_1 t - \varphi_{ch}\right] + \frac{1}{2} I_{cq} m_{gh} \cos\left[(h-1)\omega_1 t - \varphi_{gh}\right] \tag{40c}$$

$$\overline{i}_{d,2h}(t) = -\frac{1}{2} m_{gh} I_{ch} \sin(2h\omega_1 t - \varphi_{gh} - \varphi_{ch}) - \frac{1}{2} m_{ch} I_{ch} \sin(2h\omega_1 t - 2\varphi_{ch}) \tag{40d}$$

$$\overline{i}_{d,h_1+h_2}(t) = -\frac{1}{2}\left(m_{c,h_1} I_{c,h_2} + m_{c,h_2} I_{c,h_1}\right)\sin\left[(h_1+h_2)\omega_1 t - \varphi_{c,h_1} - \varphi_{c,h_2}\right] - \frac{1}{2} m_{g,h_1} I_{c,h_2} \sin\left[(h_1+h_2)\omega_1 t - \varphi_{g,h_1} - \varphi_{c,h_2}\right] - \frac{1}{2} m_{g,h_2} I_{c,h_1} \sin\left[(h_1+h_2)\omega_1 t - \varphi_{g,h_2} - \varphi_{c,h_1}\right], h_1 < h_2 \tag{40e}$$

$$\overline{i}_{d,h_2-h_1}(t) = -\frac{1}{2}\left(m_{c,h_1} I_{c,h_2} - m_{c,h_2} I_{c,h_1}\right)\sin\left[(h_2-h_1)\omega_1 t + \varphi_{c,h_1} - \varphi_{c,h_2}\right] - \frac{1}{2} m_{g,h_1} I_{c,h_2} \sin\left[(h_2-h_1)\omega_1 t + \varphi_{g,h_1} - \varphi_{c,h_2}\right] + \frac{1}{2} m_{g,h_2} I_{c,h_1} \sin\left[(h_2-h_1)\omega_1 t + \varphi_{c,h_1} - \varphi_{g,h_2}\right], h_1 < h_2 \tag{40f}$$

Substituting these equations into Eq.(28), we get:

$$\overline{v}_{dc,r} = \overline{v}_{dc,2} + \sum_{h=2}^{H}\overline{v}_{dc,h+1} + \sum_{h=2}^{H}\overline{v}_{dc,h-1} + \sum_{h=2}^{H}\overline{v}_{dc,2h} + \sum_{\substack{h_1,h_2=2 \\ h_1<h_2}}^{H}\overline{v}_{dc,h_1+h_2} + \sum_{\substack{h_1,h_2=2 \\ h_1<h_2}}^{H}\overline{v}_{dc,h_2-h_1} \tag{40}$$

where

$$\overline{v}_{dc,2}(t) = -\frac{m_e + m_q}{4\omega_1 C_{dc}} I_{cq} \cos 2\omega_1 t \tag{41a}$$

$$\overline{v}_{dc,h+1}(t) = \frac{(m_e + m_q) I_{ch} + m_{ch} I_{cq}}{2C_{dc}(h+1)\omega_1}\sin\left[(h+1)\omega_1 t - \varphi_{ch}\right] + \frac{m_{gh} I_{cq}}{2C_{dc}(h+1)\omega_1}\sin\left[(h+1)\omega_1 t - \varphi_{gh}\right] \tag{41b}$$

$$\overline{v}_{dc,h-1}(t) = \frac{-(m_e + m_q) I_{ch} + m_{ch} I_{cq}}{2C_{dc}(h-1)\omega_1}\sin\left[(h-1)\omega_1 t - \varphi_{ch}\right] + \frac{m_{gh} I_{cq}}{2C_{dc}(h-1)\omega_1}\sin\left[(h-1)\omega_1 t - \varphi_{gh}\right] \tag{41c}$$

$$\overline{v}_{dc,2h}(t) = \frac{m_{gh} I_{ch}}{4h\omega_1 C_{dc}}\cos\left(2h\omega_1 t - \varphi_{gh} - \varphi_{ch}\right) + \frac{m_{ch} I_{ch}}{4h\omega_1 C_{dc}}\cos\left(2h\omega_1 t - 2\varphi_{ch}\right) \tag{41d}$$

$$\overline{v}_{dc,h_1+h_2}(t) = \frac{m_{c,h_1} I_{c,h_2} + m_{c,h_2} I_{c,h_1}}{2C_{dc}(h_1+h_2)\omega_1}\cos\left[(h_1+h_2)\omega_1 t - \varphi_{c,h_1} - \varphi_{c,h_2}\right] + \frac{m_{g,h_1} I_{c,h_2}}{2C_{dc}(h_1+h_2)\omega_1}\cos\left[(h_1+h_2)\omega_1 t - \varphi_{g,h_1} - \varphi_{c,h_2}\right] + \frac{m_{g,h_2} I_{c,h_1}}{2C_{dc}(h_1+h_2)\omega_1}\cos\left[(h_1+h_2)\omega_1 t - \varphi_{g,h_2} - \varphi_{c,h_1}\right] \tag{41e}$$

$$\overline{v}_{dc,h_2-h_1}(t) = \frac{m_{g,h_1} I_{c,h_2}}{2C_{dc}(h_2-h_1)\omega_1}\cos\left[(h_2-h_1)\omega_1 t + \varphi_{g,h_1} - \varphi_{c,h_2}\right] + \frac{m_{c,h_1} I_{c,h_2}}{2C_{dc}(h_2-h_1)\omega_1}\cos\left[(h_2-h_1)\omega_1 t + \varphi_{c,h_1} - \varphi_{c,h_2}\right], h_1 < h_2 \tag{41f}$$

VIII. Experimental Validation and Discussions

To validate the theoretical analysis, experimental results of the LCL-type APF are presented. The system paramters are L_g=50μH, L_c=250μH, C_{dc}=20000μF, C_f=10μF, R_f=0.3 Ohm, v_s=220V (RMS). The current loop control technique and dc-link regulation are consistent with the scheme in [4]. In this study, two experimental tests are implemented, one is for constant reactive current generation, another is for compensation of nonlinear current generated by thyristor rectifer load.

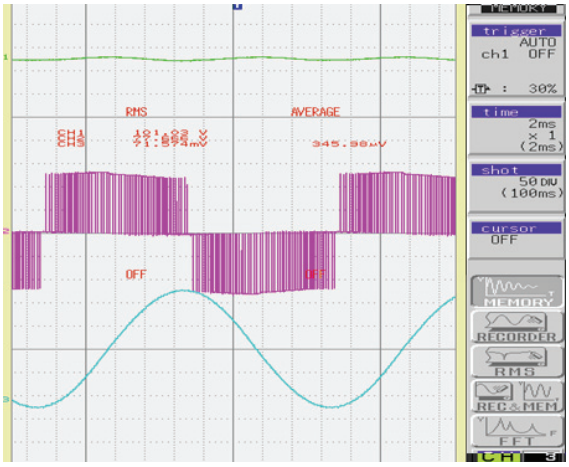

Fig.5 The experimental results of the LCL-type APF when a constant reactive current is generated.

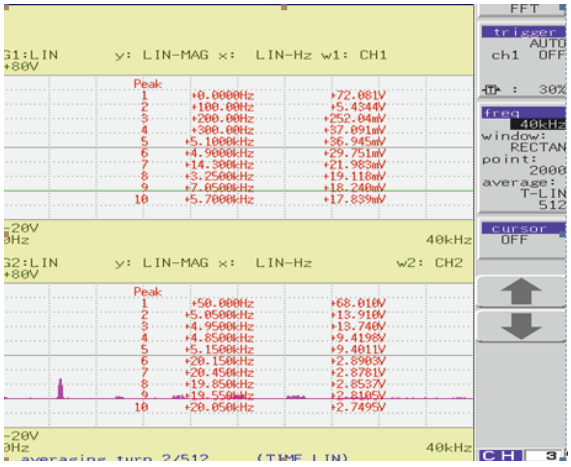

Fig.6 The FFT spectrum of the inverter dc-link voltage and the inverter output voltage.

Fig.5 shows the experimental results of the LCL-type APF when a constant reactive current is generated. The ch-1 and ch-2 in Fig.5 represents the dc-link voltage of the inverter and the inverter output voltage. The ch-3 shows

the waveform of the grid side current, which is 90 degree lagging the inverter output voltage. Fig.6 shows the FFT spectrum of the dc-link voltage and inverter output voltage. It shows that, the second order harmonic dominates the dc-link voltage, and the highest swiching ripple of the inverter output voltage is around 5kHz, which is double the switching frequency of the inverter (2.5kHz).

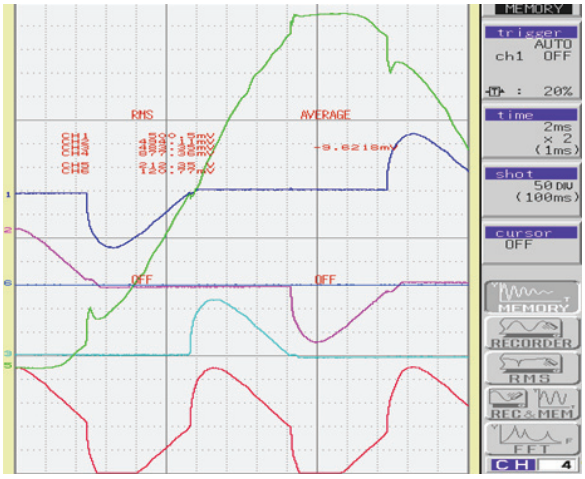

Fig.7 The experimental results of the nonlinear load currents and grid voltage when APF is turned off.(ch-1,2,3,4 corresponds to phase ‘a’, ‘b’, ‘c’, ‘N’.)

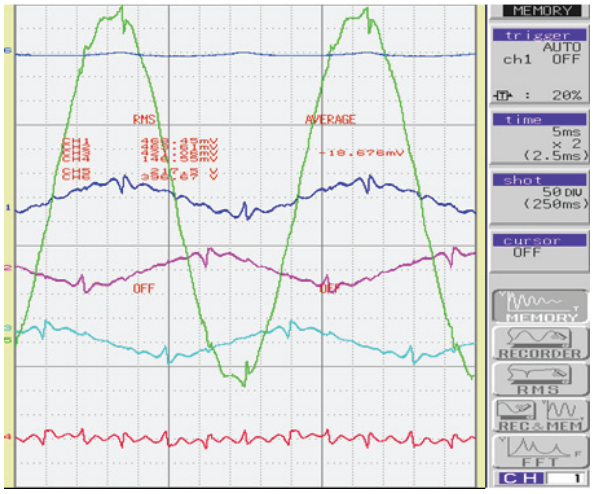

Fig.8 The experimental results of the grid currents, grid voltage and inverter dc-link voltage when APF is turned on. (ch-1,2,3,4 corresponds to phase ‘a’, ‘b’, ‘c’, ‘N’, ch-5, 6 corresponds to the grid voltage and inverter dc-link voltage.)

Figs.7-9 shows the experimental results of the LCL-type APF for nonlinear current compensation using three single-phase configuration. Fig.7 shows the waveforms of the nonlinear load currents and the grid voltage in phase ‘A’. It can be noticed that the load currents are highly nonlinear, with a characteristic harmonic component of the order 3, 5, 7, etc. And the grid voltage shows obvious notch at the conduction instant of the thyristor rectifier. Fig.8 shows the waveforms of the grid currents and grid voltage in phase ‘A’ when the APF starts compensation. It shows that the the selected harmonc components are well compenated by the APF. Fig.9 shows the FFT spectrum of the grid voltage and the inverter dc-link voltage. It shows that the switching ripple componets are well damped in the grid voltage and the dc-link voltage (ch-6) shows the fluctation of second order harmonic component, which is consistent with the theoretical analysis.

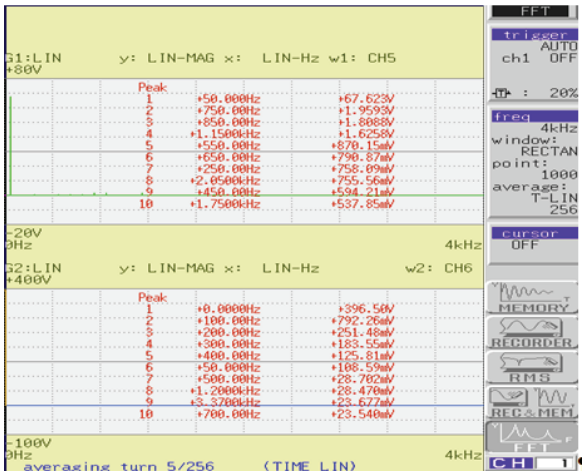

Fig.9 The FFT spectrum of the grid voltage (ch-5) and inverter dc-link voltage (ch-6).

IX. Conclusions

This paper presents the averaged and switching function modelling for the active power filter with LCL-type coupling impedance. The mathematical model of the LCL-type APF is derived using switching function modelling technique. And the equivalent circuits are derived from the averaged and switching ripple model. Besides, the ac-side and dc-side averaged and switching models of the inverter are also derived. The presented technique is extended to the analysis of the modulation signal and the inverter dc-link voltage. Finally, the experimental results are also provided, which validates the theoretical derivations.

REFERENCES

[1] Han Y., Xu L., Yao G., Zhou LD., Khan MM., Chen C., A novel modulation scheme for dc-voltage balancing control of cascaded H-bridge multilevel APF, *Przeglad Elektrot.*, 85(2009), n. 5, 81-85.

[2] Han Y., Xu L., Yun WJ., Yao G., Zhou LD., Khan MM., Chen C., Power quality enhancement for automobile factory electrical distribution system-strategies and field practice, *Przeglad Elektrot.*, 85(2009), n. 6, 159-163

[3] Han Y., Xu L., Yao G., Zhou LD., Khan MM., Chen C., Power system harmonic estimation scheme based on Affine projection adaptive filter theory, *Przeglad Elektrot.*, 85(2009), n. 11, 45-50.

[4] Han Y., Xu L., Yao G., Zhou L., Khan MM, Chen C., A Robust Deadbeat Control Scheme for Active Power Filter with LCL Input Filter, *Przeglad Elektrot.*, 86(2010), n.2, 14-19.

[5] Han Y., Xu L., Khan MM, Chen C., Yao G., Zhou L., Modelling and controller synthesis of a hybrid-LCL APF for power quality conditioning applications, *Przeglad Elektrot.*, 86(2010), n.9, 326-333.

[6] Han Y., Xu L., Yao G., Zhou L., Khan MM, Chen C., State-Space Averaging (SSA) Technique for Modeling of the Cascaded H-Bridge Multilevel DSTATCOMs and Active Filters, *International Review of Electrical Engineering-IREE*, 4(2010), n.5, 744-760.

***Authors**: Dr. Yang Han is with the Department of Power Electronics, School of Mechatronics Engineering, University of Electronic Science and Technology of China (UESTC), No.2006 XiYuan Road, West Park of Chengdu High-Tech Zone, 611731, Chengdu, P. R. China, E-mail: hanyang_facts@hotmail.com;*
Dr. Lin Xu is with the department of electrical engineering, Shanghai JiaoTong University, #800 DongChuan Road, Shanghai, P.R.China,E-mail:xulin198431@hotmail.com.